Arabian Journal of Chemistry (2022) **15**, 104371

King Saud University

Arabian Journal of Chemistry

www.ksu.edu.sa
www.sciencedirect.com

ORIGINAL ARTICLE

Theoretical and experimental study on Chloroquine drug solubility in supercritical carbon dioxide via the thermodynamic, multi-layer perceptron neural network (MLPNN), and molecular modeling

Nedasadat Saadati Ardestani [a,b], Mitra Amani [c], Maria Grishina [d], Saeed Shirazian [d,*]

[a] *Nanotechnology Research Center, Research Institute of Petroleum Industry (RIPI), P.O. Box: 14857-336, Tehran, Iran*
[b] *Department of Chemical Engineering, Tarbiat Modares University, P.O. Box: 14115-111, Tehran, Iran*
[c] *Department of Chemical Engineering, Islamic Azad University, Robat Karim Branch, 37616-16461 Robat Karim, Iran*
[d] *Laboratory of Computational Modeling of Drugs, South Ural State University, 76 Lenin Prospekt, 454080 Chelyabinsk, Russia*

Received 1 August 2022; accepted 13 October 2022
Available online 19 October 2022

KEYWORDS

Drug solubility;
Molecular modeling;
Thermodynamics;
Supercritical solvent;
Nanomedicine

Abstract The design and development of supercritical carbon dioxide (sc-CO_2) based processes for production of pharmaceutical micro/nanoparticles is one of the interesting research topics of pharmaceutical industries owing to its attractive advantages. The solubility of drugs in sc-CO_2 at different temperatures and pressures is an essential parameter which should be determined for this purpose. Chloroquine as a traditional antirheumatic and antimalarial agent is approved as an effective drug for the treatment of Covid-19. Pishnamazi *et al.* (2021) measured the solubility of this drug in sc-CO_2 at the pressure range of 120–400 bar and temperature range of 308–338 K, and correlated the obtained data using some empirical models. In this work, a comprehensive computational approach was developed to more accurately study the supercritical solubility of Chloroquine. The thermodynamic models include two equations-of-state based models (Peng-Robinson and Soave-Redlich-Kowang) and two activity coefficient-based models (modified Wilson's and UNIQUAC)), as well as, a multi-layer perceptron neural network (MLPNN)) were used for this purpose. Also, molecular modeling was performed to study the electronic structure of Chloroquine and identify the potential centers of intermolecular interactions during the dissolution process. According to the obtained results, all of the theoretical models can predict Chloroquine solubility in sc-CO_2 with acceptable

* Corresponding author.
E-mail address: shirazians@susu.ru (S. Shirazian).
Peer review under responsibility of King Saud University.

Production and hosting by Elsevier

https://doi.org/10.1016/j.arabjc.2022.104371

Nomenclature

$AARD\%$	Average absolute relative deviation
$\boldsymbol{a}(\boldsymbol{T})$	Energy parameter of the cubic EoS ($Nm^4\ mol^{-2}$)
b	Volume parameter for equations of state ($m^3\ mol^{-1}$)
f_2^L	The fugacity of the solid solute in the supercritical phase
f_2^s	The fugacity of the solute in the solid phase
H_f	Molar heat of fusion($kJ.mol^{-1}$)
g^E	Excess Gibbs free energy
k_{ij}	Binary interaction parameters in the mixing rules
l_{ij}	Binary interaction parameters in the mixing rules
MSR	Mean square regression
MSE	Mean square residual
N	Number of data points, dimensionless
P_{sub}	Sublimation pressure (Pa)
Q	Number of independent variables
R^2	Correlation coefficient
R_{adj}	Adjusted correlation coefficient
S	Equilibrium solubility
SS_E	Error sum of squares
SS_T	Total sum of squares
SS_R	Regression sum of squares
$\boldsymbol{T_c}$	Critical temperature
v^s	Solid molar volume
vdW2	Van der Waals mixing rule with two adjustable parameters
y	Mole fraction solubility
Z	Number of adjustable parameters
r	Volume parameter of the UNIQUAC model
q	surface area of the UNIQUAC model

Greek symbols

α(Tr, ω)	Temperature-dependent function in the attractive parameter of the EoS
φ	Fugacity coefficient
ω	Acentric factor
α	Regressed parameters of the Wilson's and UNIQUAC models
β	Regressed parameters of the Wilson's and UNIQUAC models
λ'	Regressed parameters of Wilson's model
Λ	Adjustable parameters
γ_2^∞	The activity coefficient of the solid solute at infinite dilution

Superscripts

cal	Calculated
exp	Experimental
i, j	Component
1	Supercritical carbon dioxide
2	Solid solute

accuracy. Among these models, the MLPNN model possesses the highest precision with the lowest average absolute relative deviation *(AARD%)* of 1.76 % and the highest R_{adj} value of 0.999.

1. Introduction

In recent decades, development of supercritical carbon dioxide (sc-CO_2) based processes in the pharmaceutical industry has attracted much attention for development of advanced pharmaceutical manufacturing. Classification of sc-CO_2 as a safe solvent by FDA (Kankala et al., 2017); significant decrement of required toxic solvents, production of high quality products without residual solvent, processing at low temperatures, and also adjustable solvation power as a function of pressure and temperature have led to widespread utilization of sc-CO_2 in various pharmaceutical processes. Among the various proposed applications, micronization/nanonization of pharmaceutical particles (e.g., solid oral dosage formulations) with desired particle attributes is one of the most important ones. The equilibrium solubility of the pharmaceutical substances in sc-CO_2 is one of the main operational parameters which should be specified for design and optimization of these processes. Accordingly, obtaining the solubility of various drug molecules in sc-CO_2 to find the suitable candidates to be processed through a sc-CO_2 based technique has become an interesting research topic (Ardestani et al., 2020; Morales-Díaz et al., 2021). However, experimental measurement of substances solubility in sc-CO_2 over a wide range of temperatures and pressures is very time consuming and requires complex and expensive apparatuses. So, thermodynamic modelling and theoretical prediction of this parameter at different operational conditions is indispensable. For this purpose, several theoretical methods including, density-based models (empirical models), equation of state (EoS) (cubic and non-cubic) based models and expanded liquid models were presented and validated. Furthermore, smart methods (e.g. artificial neural network (ANN)) (Rezaei et al., 2022) and machine Learning Models (Najmi et al., 2022) were also used to correlate the solubility of solids in sc-CO_2 with acceptable accuracy.

Empirical models were proposed for correlation of solubility data and shown to be facile methods (Faress et al., 2022). However, these models are directly interrelated with the experimental solubility data and their adjustable parameters should be determined according to experimental values (Ali Sajadian et al., 2022).

In the equation of state-based theories, supercritical carbon dioxide is considered as a condensed phase (solvent phase) and calculations is basically carried out according to the fugacity coefficient of the solute, i.e., the drug substances (Ali Sajadian et al., 2022). Equation of states are classified as, (*i*) cubic EoS in which the pressure can be written as a cubic function of molar volume (e.g. Peng-Robinson (PR) (Peng and Robinson, 1976) and Soave- Redlich-Kowang (SRK) (Soave, 1972), and (*ii*) non cubic EoS which are based on statistical associating fluid theory (SAFT) (e.g. Perturbed-Chain Polar Statistical Associating Fluid Theory (PCP-SAFT) (Gross, 2005).

Unlike these models, in expanded liquid theories such as UNIQUAC method (Nasri et al., 2012) and modified Wilson's models (Nasri, 2018), sc-CO_2 is regarded as an expanded liquid, due to prox-

imity of its density to the liquids density (Higashi et al., 2001). Accordingly, this modelling is performed according to activity coefficient of the solute. Both of equation of state and expanded liquid-based models need critical properties, molar volume and the sublimation pressure of the solute. Generally, these properties are not known for complex solute molecules and their experimental measurement is not always possible. So, various group contribution (GC) methods have been suggested for their estimation and therefore, the accuracy of the applied correlation significantly depends to the used GC method.

The artificial neural network (ANN) is a plain powerful tool to model and optimize the various processes. So, its application as a practical modelling tool in various computational engineering projects has received much attention, because of its ability for solving the complex problems. Indeed, no requirement to a mathematical model, capability in representing the complicated relation between the input and output parameters, and also learning from the experiences and interpolating the results, even for the case of incomplete inputs, are the main outstanding features of the ANN models compared to the standard computing methods (Lashkarbolooki et al., 2011; Vaferi et al., 2013).

Chloroquine ($C_{18}H_{26}ClN_3$), with the chemical structure shown in Fig. 1, is a traditional antirheumatic and antimalarial agent with antivirus and anti-inflammatory effects. It has also been confirmed that Chloroquine can be prescribed as an efficient drug for the therapy of Covid-19 patients by inhibiting the replication of the corona virus and preventing it from entering into the cells (Liu et al., 2020). However, some adverse digestive problems such as dysgeusia, dyspepsia, nausea and stomach pain, as well as other side effects like headache, ocular disorder and serious heart rhythm abnormalities have been reported for this medicine (Ponticelli and Moroni, 2017). As has been proven for most of the drugs (Amani et al., 2021; Türk, 2016; Abuzar et al., 2018), reducing the Chloroquine particles size to micro/nano scale can significantly enhance its dissolution rate and bioavailability and reduce drug dosage, leading to mitigation of these complications for patients. Therefore, enhancing the solubility of Chloroquine by nanonization technique is a very attractive task.

Pishnamazi *et al.* (Pishnamazi et al., 2021) determined the solubility of Chloroquine in sc-CO_2 at the various pressures of 120–400 bar and temperatures of 308–338 K. It was obtained in the range of 1.64×10^{-5} to 8.92×10^{-4} in terms of mole fraction. Also, they correlated the obtained solubility data via some empirical models (Kumar & Johnston (KJ), Mendez-Santiago-Teja (MST), Chrastil, Bartle *et al.*, and Garlapati & Madras models).

In the present work, the ability and accuracy of other well-known theoretical models to correlate these experimental data were investigated. For this purpose, two cubic EoSs (PR and SRK), two expanded liquid models (UNIQUAC and modified Wilson's models), and the ANN model were applied. Furthermore, Chloroquine solubility in sc-CO_2 was also studied by molecular-level computations to understand the interactions between the solute and solvent. Indeed, the molecular modeling was performed to study the electronic structure of Chloroquine and identify the potential centers of intermolecular interactions during the dissolution and crystal formation processes. Then, the predictability and accuracy of these methods for prediction of Chloroquine solubility in sc-CO_2 was evaluated through calculating some statistical parameters such as average absolute relative deviation *(AARD%)*, adjusted correlation coefficient (R_{adj}) and *F value*. The obtained results can be used to correlate the Chloroquine solubility at different conditions and minimizing the cost and time of the experimental solubility measurement.

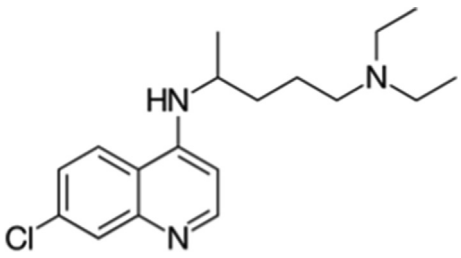

Fig. 1 Chemical structure of Chloroquine.

2. Experimental

The data used in this work are the solubility of Chloroquine in supercritical solvent (CO_2) which was measured using the gravimetric method in a PVT cell. The experimental setup used in this work is schematically indicated in Fig. 2. The system of measurement is made of two separate sections including the compression of solvent and the PVT cell for measuring the solubility values. The detailed description of the measurements are reported elsewhere (Pishnamazi et al., 2021).

3. Thermodynamic modeling

In thermodynamic relations used for theoretical solubility prediction, sc-CO_2 (solvent) and the solid solute (drug) were considered as components 1 and 2, respectively. The required physical and critical properties of the Chloroquine is not known and should be estimated by the appropriate group contribution modeling approaches. Its sublimation pressure ($P_2^{sub}(T)$), molar volume (v_2^s) and acentric factor (ω) are computed via Ambrose-Walton corresponding states method (Bruce et al., 2001), Immirzi method (Immirzi and Perini, 1977), and Constantinou-Gani method (Constantinou and Gani, 1994), respectively. Other Chloroquine properties such as boiling point (T_b), melting point (T_m), critical temperature (T_c) and critical pressure (P_c) were calculated by Marrero and Gani contribution method (Marrero and Gani, 2001). All of these properties were reported in Table 1. In all of the considered models, $R\ (8.314\ J\ mol^{-1}\ K^{-1})$, $T\ (K)$, $T_r\ (T/T_c)$, and $P\ (MPa)$ denote as the ideal gas constant, temperature, reduced temperature, and pressure, respectively. Also, solubility of the Chloroquine (solute) in sc-CO_2 (solvent) was considered as its equilibrium mole fraction (y_2).

3.1. Cubic equation of state (EoS) based models (SRK-EoS & PR-EoS)

The relations of these EoSs were shown in Table 2. These are the most commonly thermodynamic models applied to correlate the solubility of different materials in sc-CO_2 (Saadati Ardestani et al., 2020; Coimbra et al., 2006; Chim et al., 2012). In two-phase (solid solute – solvent) equilibrium condition, the fugacity coefficient of the solute in both phases should be equal. Accordingly, the equilibrium solubility (y_2) in sc-CO_2 was obtained as the following (Saadati Ardestani et al., 2020):

$$y_2 = \frac{P_2^{sub}(T)}{P} \frac{\varphi_2^{sat,s}(T)}{\varphi_2(T,P,y)} \exp\left[\frac{v_2^s(P - P_2^{sub}(T))}{RT}\right] \quad (1)$$

Because of the very small sublimation pressure obtained for Chloroquine (Table 1), its saturation fugacity coefficient ($\varphi_2^{sat,s}(T)$) can be assumed to be one. Furthermore, $\phi_2(T,P,y)$ is the fugacity coefficient of the solute in sc-CO_2, which in this study was computed through SRK-EoS (Soave, 1972), and PR-EoS (Peng and Robinson, 1976), via the following relationship (Saadati Ardestani et al., 2020):

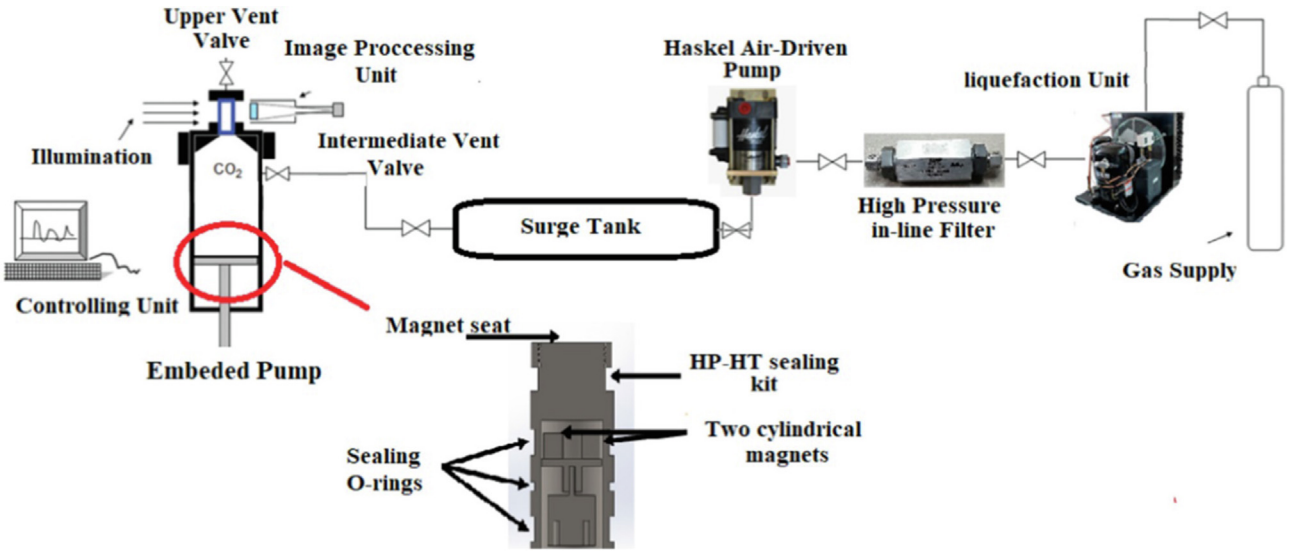

Fig. 2 Experimental setup used for measuring Chloroquine solubility in supercritical CO_2 (Pishnamazi et al., 2021). Reprinted from (Pishnamazi et al., 2020) with permission from Elsevier.

Table 1 Molecular weight and estimated physic-chemical properties of Chloroquine.

Component	MW (kg kmol^{-1})	T_b (K)	T_m (K)	T_c (K)	P_c (bar)	ω	v_s (cm^3 mol^{-1})	T (K)			
								308	318	328	338
								$P^{sub} \times 10^4$ (Pa)			
Chloroquine	319.87	676	370	917	16.5	0.47	209.3	3.8	11.5	32.4	84.6

Table 2 The relations of the PR-EoS and SRK-EoS.

Model	Equation of state	a(T)	b
Peng Robinson (PR) (Peng and Robinson, 1976)	$P = \frac{RT}{v-b} - \frac{a(T)}{v\,(v+b)+b\,(v-b)}$	$a(T) = \frac{0.45724R^2\,T_c^2}{P_c} \times \alpha(T_{r,\omega})$ $\alpha(T_{r,\omega}) = [1 + k(1 - T_r^{0.5})]^2$ $k = 0.37464 + 1.54226\omega - 0.26992\omega^2$	$b = \frac{0.07780\,R\,T_c}{P_c}$
Soave–Redlich–Kwong (SRK) (Soave, 1972)	$P = \frac{RT}{v-b} - \frac{a(T)}{v\,(v+b)}$	$a(T) = \frac{0.42747R^2\,T_c^2}{P_c} \times \alpha(T_{r,\omega})$ $\alpha(T_{r,\omega}) = [1 + m(1 - T_r^{0.5})]^2$ $m = 0.480 + 1.574\omega - 0.176\omega^2$	$b = \frac{0.08664RT_c}{P_c}$

$$RT \ln \varphi_i = -RT \ln Z + \int_V^\infty \left[\left(\frac{\partial P}{\partial n_i} \right)_{T,V,n_j \neq n_i} - \frac{RT}{V} \right] dV \qquad (2)$$

where Z, V and n_i are the compressibility factor, the molar volume of sc-CO_2 and the moles number of species i, respectively.

3.2. Expanded liquid models (UNIQUAC and modified Wilson's models)

Equality of the solute fugacity in the solid phase (f_2^S) with its value in the sc-CO_2 phase (liquid solvent) ($f_2^{L=Sc-CO_2}$) is the thermodynamic criteria used for describing the equilibrium condition between the solute and sc-CO_2. According to insolubility of sc-CO_2 in the solid solute, f_2^S is equal to fugacity of the pure solute($f_2^{\theta S}$). The term of (f_2^L) is described based on the solute activity coefficient(γ_2), as follows (Ali Sajadian et al., 2022):

$$f_2^L = f_2^{\theta S} = \gamma_2 y_2 f_2^{\theta L} \qquad (3)$$

where, $f_2^{\theta L}$ is the fugacity of the pure solute in sc-CO_2 phase (expanded liquid phase). Regardless the change of solute heat capacity (Δc_p) and regarding the infinite dilution condition due to little dissolution of the solid solute in sc-CO_2 (Nasri et al., 2013), the proposed Prausnitz relation (Prausnitz et al., 1998) between $f_2^{\theta L}$ and $f_2^{\theta S}$ can be summarized as the following (Ali Sajadian et al., 2022):

$$y_2 = \frac{1}{\gamma_2^\infty} \exp\left(\frac{-\Delta H_2^f}{R} \left(\frac{1}{T} - \frac{1}{T_m} \right) \right) \qquad (4)$$

Here, γ_2^{∞} ΔH_2^f and T_m are the activity coefficient of the solid solute at the infinite dilution condition, heat of fusion and melting point of the solute, respectively. In this study, the term of γ_2^{∞} was specified via the modified Wilson's model (Nasri, 2018) and UNIQUAC model.

3.2.1. Modified Wilson's model

Correlating the solubility of different materials in sc-CO_2 through the Wilson's model has been previously performed by several researchers such as, Nasri (2018), Nasri et al. (2013); Pitchaiah et al. (2019), Pitchaiah et al. (2018); Narayan et al. (2015), and Reddy and Madras (2013), Reddy and Madras (2012). Wilson's equation includes a combinatorial contribution part based on Flory's theory, and another part based on the Gibbs excess energy(G^E), as follows (Nasri, 2018):

$$\frac{G^E}{RT} = -y_1 ln(y_1 + y_2\Lambda_{12}) - y_2 ln(y_1\Lambda_{21} + y_2) \tag{5}$$

where, Λ_{12} and Λ_{21} are the dependent adjustable parameters to the sc-CO_2 molar volume (υ_1), the solid solute molar volume (υ_2), and the interaction energy (λ) between them (Nasri, 2018):

$$\Lambda_{12} \equiv \frac{\upsilon_2}{\upsilon_1} exp\left(-\frac{\lambda_{12} - \lambda_{11}}{RT}\right) \tag{6}$$

$$\Lambda_{21} \equiv \frac{\upsilon_1}{\upsilon_2} exp\left(-\frac{\lambda_{21} - \lambda_{22}}{RT}\right) \tag{7}$$

Through differentiation of Eq. (5) and rearrangement of the obtained function, the term of γ_2 can be determined by the following relation (Nasri, 2018):

$$ln\gamma_2 = -ln(y_2 + y_1\Lambda_{21}) - y_1\left[\frac{\Lambda_{12}}{y_1 + y_2\Lambda_{12}} - \frac{\Lambda_{21}}{y_2 + y_1\Lambda_{21}}\right] \tag{8}$$

At the infinite dilution condition, this relation can be summarized to the form of Eq. (9) (Assael et al., 1996), in which Λ_{12} and Λ_{21} are written in reduced form, as follows (Nasri, 2018):

$$\ln \gamma_2^{\infty} = 1 - \underbrace{v_2\rho \exp\left(-\frac{\lambda'_{12}}{T_r}\right)}_{\Lambda_{12}} - \ln\underbrace{\left(\frac{1}{v_2\rho}\exp\left(-\frac{\lambda'_{21}}{T_r}\right)\right)}_{\Lambda_{21}} \tag{9}$$

where, ρ is the sc-CO_2 density and, $\lambda'_{12}(=\frac{\lambda_{12}}{RT_c})$and $\lambda'_{12}\left(=\frac{\lambda_{21}}{RT_c}\right)$are the dimensionless interaction energies. Nasri (Nasri, 2018) defined a simple expression for definition the term of υ_2 (Nasri, 2018):

$$\upsilon_2 = \alpha\rho_r + \beta \tag{10}$$

Finally, α, β, λ'_{12} and λ'_{12} are the parameters of the Wilson's model specified through regression. The term of $\rho_r\ (=\frac{\rho}{\rho_c})$ is the reduced density of the solvent (sc-CO_2), in which ρ_c is the critical sc-CO_2 density (kg.m^{-3}).

3.2.2. UNIQUAC model

Predicting the solubility of various components in sc-CO_2 via the UNIQUAC model has been previously reported by Nasri et al. (2012), Nasri et al. (2013), Loubna et al. (2014), Zhao et al. (2020), Chang and Morrell (1985), and Sodeifian et al. (2020), Sodeifian et al. (2020). Considering the size and nature of the molecules, as well as the intermolecular forces between the solute and solvent molecules are the strengths of this model. Furthermore, it can be exploited to solutions containing small or large molecules, such as polymers (Nasri et al., 2013). In the UNIQUAC model, γ_2^{∞} includes a combinatorial contribution part to describe the main entropic contribution($\gamma_2^{c,\infty}$), and a residual part ($\gamma_2^{R,\infty}$) to indicate intermolecular forces which are cause of the mixing enthalpy (Prausnitz et al., 1998):

$$ln\gamma_2^{\infty} = ln\gamma_2^{c,\infty} + ln\gamma_2^{R,\infty} \tag{11}$$

The term of $\gamma_2^{c,\infty}$ is a function of composition and structure of the molecules, and its determination requires only the pure component data, while the parameter of $\gamma_2^{R,\infty}$ depends to the intermolecular forces (Prausnitz et al., 1998):

$$\ln\gamma_2^{c,\infty} = 1 - \frac{r_2}{r_1} + \ln\frac{r_2}{r_1} - q_2\frac{z}{2}\left(1 - \frac{r_2q_1}{r_1q_2} + \ln\frac{r_2q_1}{r_1q_2}\right) \tag{12}$$

$$\ln\gamma_2^{R,\infty} = q_2\frac{\alpha'_{12}}{T_r} + q_2\left(1 - e^{-\frac{\alpha'_{21}}{T_r}}\right) \tag{13}$$

To account for the influence of T and P, the parameters are expressed as (Prausnitz et al., 1998):

$$\alpha'_{12} = \alpha_{12}\,\rho_r^{\beta_{12}}\ \&\ \alpha'_{21} = \alpha_{21}\,\rho_r^{\beta_{21}} \tag{14}$$

where $\alpha_{12}, \alpha_{21}, \beta_{12}$ and β_{21} are the parameters of the model.

4. Multilayer perception neural network (MLPNN)

This model was developed based on the way of information processing in the human brain. Learning happens in an interconnected network of the brain biological neurons, which can suggest an alternative way to solve the complicated problems. The ANN model is based on repetitive, known and predictable patterns of the input data to be able to provide logical and correct answers in the output. Neural network with repetition and storage of experimental data and their complete knowledge and finally good and complete training by the experimental data can turn network inputs into correct responses with low error. For modeling using ANN, a dataset of measured data is needed to build the model (Amani, 2021).

In an ANN, a neuron executes two functions: tan-sigmoid transfer function *(Tansig)* and linear transfer function *(purelin)*. In the ANN algorithm, weighted inputs and bias values are added together and uses *Tansig* function to quickly train the network. Then, a suitable and specific scalar output is obtained by *purelin* function at the output layer. The ANN is composed of neurons arranged in three layers, one input layer which receives the experimental information and parameters, one output layer, which produces the calculated values of the dependent variable, and at least one hidden layer between the previous two layers. All of these layers posse a group of computing neurons, in which the number of neurons in the input and output layers are specified by the system's characteristics, while their number in the hidden layer is an adjustable parameter, which should be optimized (Bakhbakhi, 2012). Accordingly, the main parts of the ANN modelling include (i) determination the input values, (ii) selection the appropriate algorithm for accurate model training, (iii) specification the

number of neurons in the hidden layer, and (iv) evaluating and validating the ANN model.

The connection template of each neuron to other neuron in the next layer is known as the network "architecture". Among the various suggested architectures, multilayer perception neural network (MLPNN) structure with the back-propagation (BP) algorithm, as the training method, is the most popular ones.

The inputs to the neuron i in hidden or output layer (Y_i) include the sum of its weighted input multiply of its weight (ω_i) in its input parameter (x_i) and its bias(θ_i), which can be shown mathematically with the following relation (Ghoreishi and Heidari, 2013):

$$Y_i = \sum_{i=1}^{n} x_i\omega_i + \theta_i \tag{15}$$

Adjustments of weights and biases are based on reducing the difference between the values of obtained data and the experimental ones. The BP algorithm consists of three steps: (i) assessment of the weights and biases and calculation of the output values, (ii) computation and back propagation of the relevant error, and (iii) variation the weights. Among the proposed BP algorithms, Levenberg-Marquardt algorithm (LMP) accompanied with the gradient descent technique was used in this work to minimize the sum square error (SSE) and mean square error (MSE). This algorithm quickly learns and uses *Tansig* and *purelin* functions at the hidden and output layers, respectively.

5. Assessment the precision of the thermodynamic and ANN models

The performance and precision of the mentioned methods was

statistically evaluated via computing the difference between the experimental data $(y_{i,\exp})$ and the calculated one$(y_{i,cal})$, known as $AARD\%$ (Saadati Ardestani et al., 2020):

$$AARD\% = \frac{1}{N}\sum_{i=1}^{n}\left|\frac{y_{i,cal} - y_{i,\exp}}{y_{i,\exp}}\right| \times 100\% \tag{16}$$

Here, N is the number of data points for each set.

The R_{adj} value is calculated by the following relationship (Saadati Ardestani et al., 2020):

$$R_{adj} = \sqrt{\left|\underbrace{1 - \frac{SS_E}{SS_T}}_{R^2} - \frac{Q(1-R^2)}{N-Q-1}\right|} \tag{17}$$

where, SS_E is the error sum of squares and SS_T is the total sum of squares. The capability of the theoretical models in fitting the real data can be determined by *F-value* parameter (Saadati Ardestani et al., 2020):

$$F - value = \frac{SS_R/Q}{SS_E/(N-Q-1)} = \frac{MSR}{MSE} \tag{18}$$

Here, SS_R, MSR and MSE denote the regression sum of squares, the mean square regression, and the mean square residual, respectively.

6. Molecular modeling

6.1. Study of the electronic structure of Chloroquine, its crystal fragment and its complexes with CO_2

Dissolution process as well as the formation of a crystal lattice, including the formation of nanoparticles, largely depends on the electronic structure of the Chloroquine. To study the electronic structure of Chloroquine and identification the potential centers of intermolecular interactions during the dissolution and crystal formation processes, AlteQ orbital-free quantum chemical method was used in this work. This method has already shown a qualitative description of the 3D electron density maps of organic and inorganic compounds, determined using high resolution low temperature X-ray diffraction analysis (Potemkin and Grishina, 2008; Grishina and Potemkin, 2019; Potemkin and Grishina, 2018). AlteQ was developed for large molecular systems, it allows the evaluation of 3D electron density maps, and this method solves a wide range of problems.

6.2. The approach for the prediction of the zones of intermolecular contacts (contact zones) using AlteQ

One of the problems is the prediction of the directions of intermolecular contacts according to the electronic structure of a molecule (molecular system). The electronic structure of Chloroquine molecule, Chloroquine crystal fragment and Chloroquine-CO_2 complexes was investigated using the approach which was previously proposed by Vladimir Potemkin *et al.* (Potemkin and Grishina, 2021). It is based on the Valence shell electron pair repulsion (VSEPR) theory (Gillespie, 1963; Gillespie and Nyholm, 1957), which assumes that electron pairs are arranged in such a way as to minimize repulsive effects of each other. Therefore, in the terms of AlteQ 3D maps of electron density, it means the determination of space points near an atom, characterized by the minimum contribution of the electron density of covalently bound ligands of the atom in the molecule (molecular system). The set of these points forms the contact zone for potential intermolecular interactions. These contact zones determine the directions of intermolecular interactions with the environment of the molecule (receptor, solvent or other Chloroquine molecules during crystal formation), affecting the structure of the crystal or non-covalently bound complexes with the receptor or solvent.

6.3. The approach for the evaluation of the overlap zones of the molecule (ligand) with the environment using AlteQ

Another task of the AlteQ method is to determine the overlap zones of a molecule (ligand) with the environment, for example, a receptor, a solvent, or with the rest of the crystal fragment. This approach is based on the analysis of AlteQ 3D maps of electron density of receptor-ligand, solvent–solute complexes or a molecule surrounded by neighbors in the crystal fragment. The approach determines the set of m points of intermolecular space with electron density value of the molecule (ligand) $\rho_{(mol)m} > 0.001 a.u.$ and electron density value of the neighbors (receptor, solvent or the rest of the crystal fragment) $\rho_{(neigbors)m} > 0.001 a.u.$ at the m points (Rimac et al.,

2020; Palko et al., 2021). Thus, these zones are simultaneously characterized by a significant value of the electron density of both the molecule and its environment; therefore, these zones are overlap zones of the molecule with the neighbors.

6.4. Modeling of the Chloroquine crystal fragment

For determination the structure of the Chloroquine crystal fragment, experimental data on the structure of the unit cell were found in the Cambridge Crystallographic Data Centre (CCDC) (Groom et al., 2016), with the database code of CCDC 1121749. Then, the fragment of the Chloroquine crystal was built by the Mercury software by packing elementary cells along a, b, and c axes in the amount of 2*2*2. An analysis of overlap zones was made for a molecule surrounded on all sides by neighboring molecules. The position of hydrogens was clarified using QM/MM technique based on orbital-free quantum chemical method AlteQ and MM3 force field.

6.5. Modeling of Chloroquine-CO_2 complexes using MOPS algorithm

The simulation of the complexes was carried out using the MOPS algorithm also based on the QM/MM technique (Shchelokov et al., Langmuir 2019). This algorithm is based on the assumption that all changes in the structure occur along the directions of atomic vibrations. Therefore, in the general case, the structure of the complex depends little on the initial arrangement of molecules in the complex relative to each other. Modeling was carried out with an explicit and a continual account of the solvent (CO_2), while the mole fraction of Chloroquine and the temperature of the process varied according to the values given in Table 3. At the same time, the phased construction of Chloroquine-xCO_2 complexes with values x = 1–6 was carried out.

7. Results and discussion

In the current work, the solubility of Chloroquine in sc-CO_2 was anticipated by different theoretical models (PR-EoS, SRK-EoS, Wilson's model, UNIQUAC model, and the ANN), as well as the molecular modeling. The precision and accuracy of the theoretical models to correlate the solubility of Chloroquine were evaluated by comparison between the obtained data and the experimental ones, reported by Pishnamazi *et al.* (Pishnamazi et al., 2021). The reported experimental solubility data at various pressures (120 to 400 bar) and temperatures (308 to 338 K), along with the calculated sc-CO_2 density was shown in Table 3.

7.1. Artificial neural network (ANN) model

To validate, test and train the ANN, the experimental solubility data of 41 pharmaceutical compounds (Pishnamazi et al., 2021; Ali Sajadian et al., 2022; Pishnamazi et al., 2020; Chim et al., 2012; Suleiman et al., 2005; Ch and Madras, 2010; Hezave et al., 2012; Zhan et al., 2014; Yamini et al., 2012; Yang et al., 2017; Pishnamazi et al., 2021; Zabihi et al., 2020; Esfandiari and Sajadian, 2022; Ciou et al., 2017; Wang et al., 2021; Zabihi et al., 2021; Xiang et al., 2019; Pishnamazi et al., 2020; Zabihi et al., 2021; Shojaee et al., 2013; Yamini and Moradi, 2011; Ardjmand et al., 2014; Asiabi et al., 2013; Khamda et al., 2013; Zeinolabedini Hezave et al., 2012; Karimi Sabet et al., 2012; Hosseini et al., 2010; Zeinolabedini Hezave and Esmaeilzadeh, 2012; Hojjati et al., 2007) were collected, shown in Table 4. 70 %, 15 %, and 15 % of these data were used for the ANN training, validation and testing of the ANN, respectively.

The schematic of the used MLPNN structure to predict the Chloroquine solubility in sc-CO_2 is shown in Fig. 3. In the current work, the input matrix (1200 × 3) was arranged with 7 parameters of pressure, temperature, molecular weight, melting point and density, and the output matrix (1200 × 1) was arranged with one variable includes the Chloroquine solubility in terms of its mole fraction.

To find the optimum number of neurons for training the network, different number of neurons were tested (23 neurons). Then, various transfer functions were tried for training the network with the optimum number of neurons in the hidden layer (Amani, 2021). The outputs illustrated that the (LMP) algorithm would propose the best results to train the ANN with 23 neurons in the hidden layer. According to Fig. 4, the best validation performance was obtained at epoch 147, which was corresponds to a MSE value of 1.2855e-05.

Table 3 Experimental values of Chloroquine solubility in sc-CO_2, reported by Pishnamazi et al. (2021).

P (bar)[a]	T (K)[a]							
	308 K		318 K		328 K		338 K	
	ρ (kg/m^3)[b]	y_2[c]	ρ (kg/m^3)[b]	y_2[c]	ρ (kg/m^3)[b]	y_2[c]	ρ (kg/m^3)[b]	y_2[c]
120	768.4	8.26×10^{-5}	659.73	4.26×10^{-5}	506.85	4.04×10^{-5}	384.17	1.64×10^{-5}
160	828.10	1.33×10^{-4}	761.07	1.13×10^{-4}	682.39	7.35×10^{-5}	593.75	5.96×10^{-5}
200	866.48	1.53×10^{-4}	813.52	1.76×10^{-4}	755.52	1.95×10^{-4}	692.68	2.22×10^{-4}
240	895.54	2.11×10^{-4}	850.10	2.26×10^{-4}	801.92	2.33×10^{-4}	751.17	2.59×10^{-4}
280	919.23	2.50×10^{-4}	878.62	3.05×10^{-4}	836.35	3.45×10^{-4}	792.59	3.87×10^{-4}
320	939.39	2.95×10^{-4}	902.22	3.78×10^{-4}	863.97	4.40×10^{-4}	824.82	5.02×10^{-4}
360	957.02	3.28×10^{-4}	922.46	4.12×10^{-4}	887.18	5.21×10^{-4}	851.34	6.04×10^{-4}
400	972.74	3.74×10^{-4}	940.24	4.55×10^{-4}	907.27	6.76×10^{-4}	873.95	8.92×10^{-4}

[a] Standard uncertainty, u, are u (T) = 0.1 K and u (P) = 0.35 bar.
[b] Density of sc-CO_2, obtained from the NIST web-book (https://webbook.nist.gov/chemistry).
[c] The equilibrium mole fraction of Chloroquine in sc-CO_2, reported by Pishnamazi *et al.* elsewhere (Pishnamazi et al., 2021).

Table 4 Experimental data used in this work to train, test, and validate the ANN.

Component	Formula	M_w (g/mol)	T range (K)	P range (bar)	Data points	T_m (K)	Solubility range	Ref.
2-phenyl-4*H*-1,3-benzoxazin-4-one	$C_{14}H_9NO_2$	223.233	308–328	100–275	23	397	0.8×10^{-4}-4.5×10^{-4}	(Suleiman et al., 2005)
Azodicarbonamide	$C_2H_4N_4O_2$	116.08	308–328	100–300	26	497	0.9×10^{-5}-2.6×10^{-5}	(Suleiman et al., 2005)
Propyphenazone	$C_{14}H_{18}N_2O$	230.31	308–328	90–190	18	376	0.38×10^{-4}-18.82×10^{-4}	(Ch and Madras, 2010)
Sulindac	$C_{20}H_{17}FO_3S$	356.41	308–338	160–400	28	456	1.05×10^{-4}-8.69×10^{-3}	(Van der Waals, 1873)
Thymidine	$C_{10}H_{14}N_2O_5$	242.23	308–328	100–275	20	460	1.2×10^{-6}-8×10^{-6}	(Suleiman et al., 2005)
5-Fluorouracil	$C_4H_3FN_2O_2$	130.077	313–323	100–200	12	555–556	1.3×10^{-6}-5.25×10^{-6}	(Zhan et al., 2014)
Docetaxel	$C_{43}H_{53}NO_{14}$	285.303	318–348	120–360	45	462	0.37×10^{-4}-7.02×10^{-4}	(Yamini et al., 2012)
Capecitabine	$C_{15}H_{22}FN_3O_6$	359.35	308–348	152–354	40	362	0.32×10^{-5}-15.88×10^{-5}	(Yamini et al., 2012)
Lenalidomide	$C_{13}H_{13}N_3O_3$	259.25	308–338	120–300	28	560.65	0.02×10^{-4}-1.08×10^{-4}	(Ali Sajadian et al., 2022)
Silymarin	C25H22O10	482.4	308–338	80–220	32	440	0.27×10^{-5}-8.01×10^{-5}	(Yang et al., 2017)
Chloroquine	$C_{18}H_{26}ClN_3$	319.87	308–338	120–400	28	370	1.64×10^{-5}-8.92×10^{-4}	(Pishnamazi et al., 2021)
Decitabine	$C_8H_{12}N_4O_4$	228.21	308–338	120–400	28	466–469	$2.84 \times 10^{-5} - 1.07 \times 10^{-3}$	(Pishnamazi et al., 2021)
Fenoprofen	$C_{15}H_{14}O_3$	242.27	308–338	120–400	28	441–444	2.01×10^{-5}- 4.2×10^{-3}	(Zabihi et al., 2020)
Glibenclamide	$C_{23}H_{28}ClN_3O_5S$	494	308–338	100–310	24	446	3×10^{-6}- 79.2×10^{-6}	(Esfandiari and Sajadian, 2022)
Warfarin	$C_{19}H_{16}O_4$	308.3	308–328	100–180	15	434	1.48×10^{-6}- 4.32×10^{-6}	(Ciou et al., 2017)
Gliclazide	$C_{15}H_{21}N_3O_3S$	323.41	308–328	100–185	18	445.9	0.126×10^{-6}- 5.01×10^{-6}	(Wang et al., 2021)
Captopril	$C_9H_{15}NO_3S$	217.28	308–328	100–185	18	382.5	0.359×10^{-5}- 9.32×10^{-5}	(Wang et al., 2021)
Salsalate	$C_{14}H_{10}O_5$	258.23	308–338	120–400	28	420	3.77×10^{-5}- 3.88×10^{-3}	(Zabihi et al., 2021)
Busulfan	C6H14O6S2	246.304	308–338	120–400	28	387–390	3.27×10^{-5}- 8.65×10^{-4}	(Pishnamazi et al., 2020)
Gambogic Acid	C38H44O8	628.7	308–328	100–300	15	361.5	0.163×10^{-5}- 2.262×10^{-5}	(Xiang et al., 2019)
Tamoxifen	C26H29NO	371.51	308–338	120–400	28	370–371	1.88×10^{-5}- 8.29×10^{-4}	(Pishnamazi et al., 2020)
Temozolomide	$C_6H_6N_6O_2$	194.1	308–338	120–400	28	485	4.3×10^{-4}- 5.28×10^{-3}	(Zabihi et al., 2021)
Piroxicam	$C_{15}H_{13}N_3O_4S$	331.35	308–338	160–400	28	473	1.17×10^{-5}- 5.12×10^{-4}	(Shojaee et al., 2013)
Ketoconazole	$C_{26}H_{28}Cl_2N_4O_4$	531	308–348	122–355	45	423	0.05×10^{-5}- 17.45×10^{-5}	(Yamini and Moradi, 2011)
Clotrimazole	$C_{22}H_{17}ClN_2$	344	308–348	122–355	45	418	0.02×10^{-5}- 10.66×10^{-5}	(Yamini and Moradi, 2011)
Ibuprofen	C13H18O2	206.28	308–318	80–130	31	349	0.015×10^{-3} to 3.261×10^{-3}	(Ardjmand et al., 2014)
Desoxycorticosterone acetate	$C_{23}H_{32}O_4$	372.497	308–348	122–355	45	430	0.09×10^{-5} to 13.93×10^{-5}	(Asiabi et al., 2013)
Clobetasole propionate	$C_{25}H_{32}ClFO_5$	466.97	308–348	122–355	45	466.97	0.01×10^{-5} to 0.35×10^{-5}	(Asiabi et al., 2013)
Cefixime trihydrate	$C_{16}H_{15}N_5O_7S_2{\cdot}3H_2O$	507.5	308–328	183–355	18	491–498	1.6×10^{-7}–3.02×10^{-7}	(Khamda et al., 2013)
Oxymetholone	$C_{21}H_{32}O_3$	332.5	308–328	183–355	18	445–453	1.6×10^{-5}–1.49×10^{-4}	(Khamda et al., 2013)
Mefenamic acid	$C_{15}H_{15}NO_2$	241.29	308–338	160–400	28	503–504	8.31×10^{-5}–5.98×10^{-3}	(Zeinolabedini Hezave et al., 2012)
Acetaminophen	$C_8H_9NO_2$	151.16	313–343	100–250	12	443	0.66×10^{-6}–9.66×10^{-6}	(Karimi Sabet et al., 2012)
Clozapine	$C_{18}H_{19}ClN_4$	326.83	318–348	121.6–354	36	456	$3.6 \times 10^{-6} - 4.2 \times 10^{-5}$	(Hosseini et al., 2010)
Lamotrigine	$C_9H_7Cl_2N_5$	256.938	318–348	121.6–354	36	491	$1 \times 10^{-6} - 6 \times 10^{-5}$	(Hosseini et al., 2010)
Diclofenac Acid	$C_{14}H_{11}Cl_2NO_2$	296.14	308–338	120–400	32	471–473	2.34×10^{-5}–1.98×10^{-3}	(Zeinolabedini Hezave and Esmaeilzadeh, 2012)
Dexamethasone	C22H29FO5	392.5	308–328	151–357	15	533–537	1.25×10^{-6}–2.81×10^{-6}	(Chim et al., 2012)
Rosuvastatin	$C_{22}H_{28}FN_3O_6S$	481.5	308–348	121.6–354.6	45	435	0.03×10^{-4}–2.44×10^{-4}	(Hojjati et al., 2007)
Simvastatin	$C_{25}H_{38}O_5$	418.5	308–348	121.6–354.6	45	408–411	0.02×10^{-4}–5.35×10^{-4}	(Hojjati et al., 2007)
Atorvastatin	$C_{33}H_{33}FN_2O_4$	540.6	308–348	121.6–354.6	45	432.2–463.7	0.01×10^{-4}–14.46×10^{-4}	(Hojjati et al., 2007)
Fluvastatin	$C_{24}H_{26}FNO_4$	411.4	308–348	121.6–354.6	45	467–470	0.05×10^{-4}–6.01×10^{-4}	(Hojjati et al., 2007)
Lovastatin	$C_{24}H_{36}O_5$	404.5	308–348	121.6–354.6	45	447.5	0.11×10^{-4}–1.14×10^{-4}	(Hojjati et al., 2007)

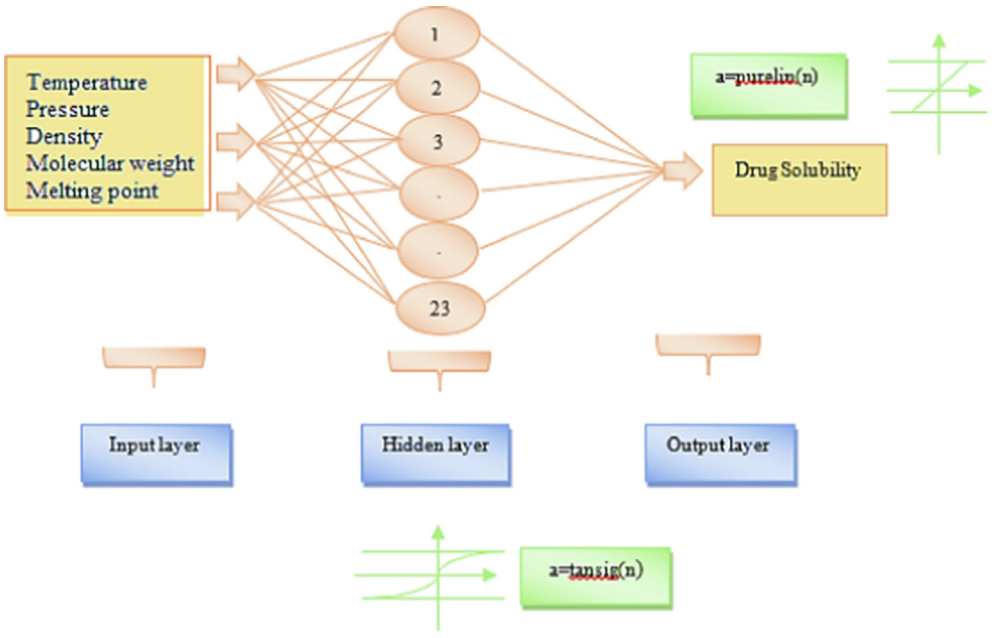

Fig. 3 The schematics of the used MLPNN structure for prediction of Chloroquine solubility in sc-CO_2.

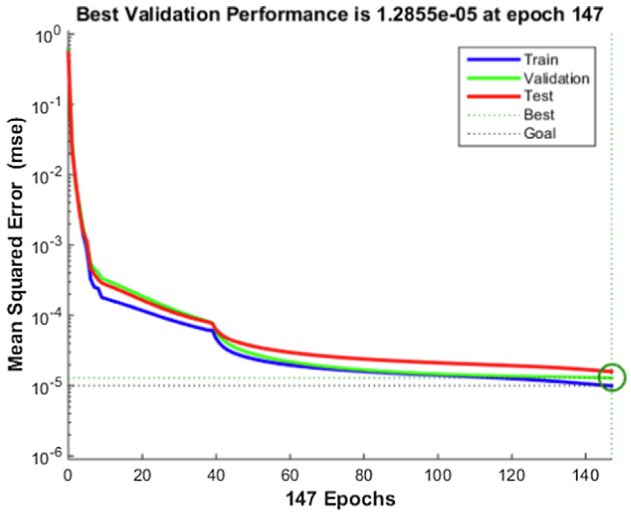

Fig. 4 Variations of the MSE with epoch during the different steps of the ANN.

Due to the dependence of the ANN performance on the initial weights that are randomly selected in the training step, the best network is characterized with the number of the iterations on this step. The final/adjusted weights matrix and the associated biases from the optimum condition are determined and the neural network (ANN) is run. So, by using a large amount of experimental data in the network, the network is well trained and has provided acceptable and appropriate results.

Fig. 5 shows the scatter diagrams compare the experimental data (target) with the ANN computed results in each step including training, validation and testing. As can be seen, the predicted solubility values are well consistent with the experimental data for all steps. The correlation coefficients (R^2) were found to be 0.99955, 0.99951, 0.99911 and 0.99955 for training, validation, testing and all data, respectively, which are totally satisfactory and acceptable. The optimal operational conditions in terms of pressure, temperature and density to obtain the maximum Chloroquine solubility in sc-CO_2 were determined with the ANN model coupled with the genetic algorithm (GA). According to the obtained results, maximum solubility of Chloroquine in terms of its equilibrium mole fraction ($y = 8.00 \times 10^{-4}$) was obtained at 338 K and 400 bar, which is in agreement with the experimental reported one ($y = 8.92 \times 10^{-4}$) (Pishnamazi et al., 2021).

7.2. Thermodynamic modeling

7.2.1. Cubic equation of states (SRK-EoS and PR-EoS)

These two cubic equation of states were frequently applied to correlate the solubility of different drugs in sc-CO_2. Also, the van der Waals (vdW) mixing rule with two binary interaction parameters (l_{ij} and k_{ij}) is the most well-known mixing rule proposed for definition the terms of $a(T)$ and b of these EoSs (Table 2), as follows (Kennedy, 2011):

$$a_m = \sum_j y_i y_j \sqrt{a_i a_j}(1 - k_{ij}) \tag{19}$$

$$b_m = \sum_j y_i y_j \frac{(b_i + b_j)}{2}(1 - l_{ij}) \tag{20}$$

The simulated annealing (SA) algorithm (Sodeifian et al., 2020) was used to determine the optimum values of the l_{ij} and k_{ij} parameters, through minimizing the $AARD\%$ value. These parameters are linear descending functions of temperature whose slope and intercept are determined by the linear regression analysis. Obtained l_{ij} and k_{ij} functions for the PR-EoS and SRK-EoS are in the form of Eq. (21) and Eq. (22), respectively. Also, these linear functions with the negative slope were indicated in Fig. 6:

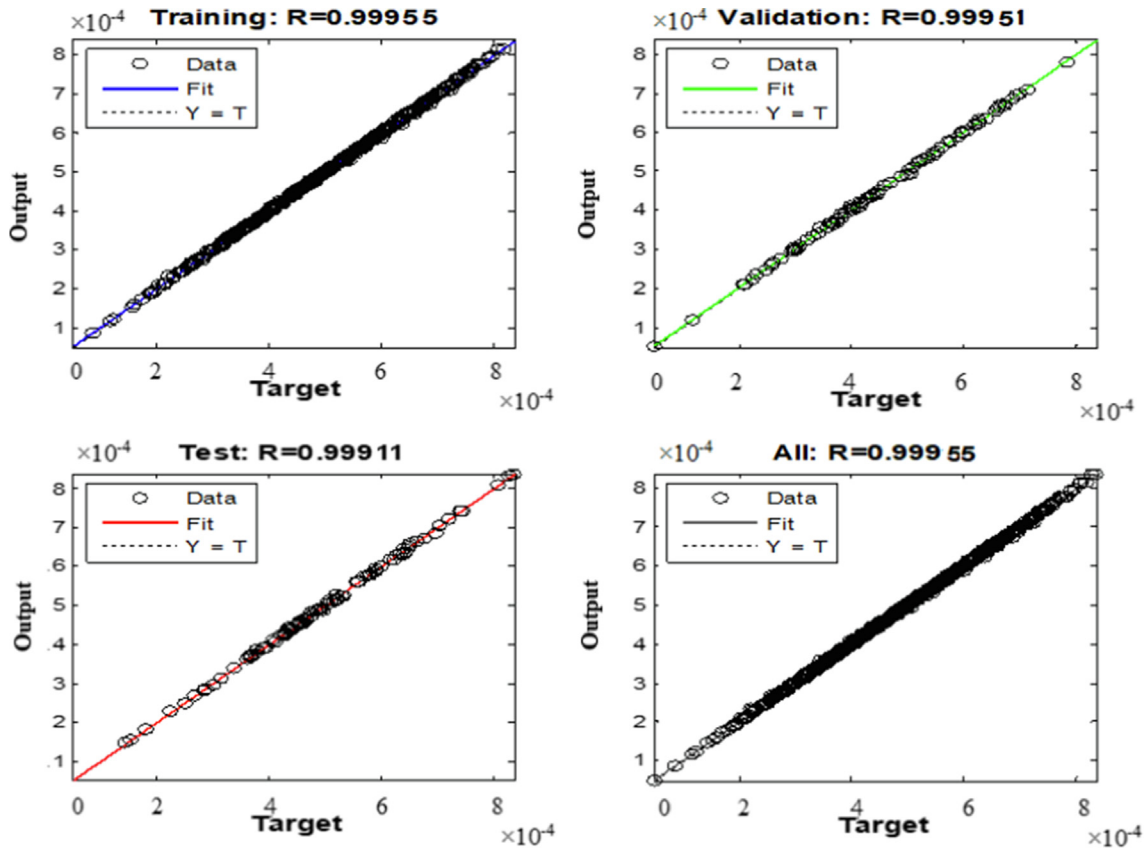

Fig. 5 Comparison between the experimental values and the output data of the ANN model during the different steps of the ANN.

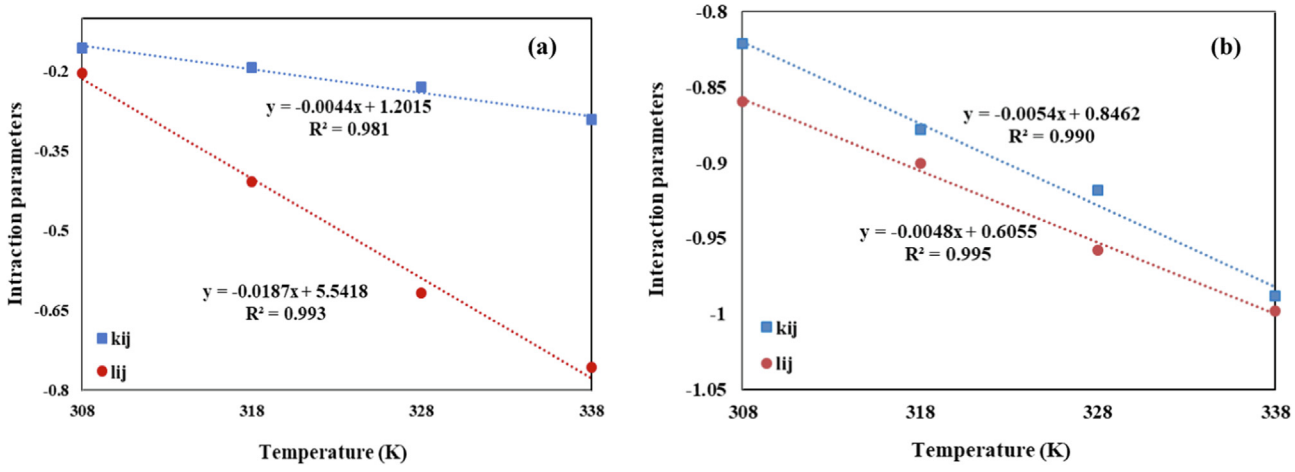

Fig. 6 Linear function of l_{ij} and k_{ij} versus the temperature (a) PR-EoS, and (b) SRK-EoS.

$$l_{ij} = -0.0187\,T + 5.5418 \quad \& \quad k_{ij} = -0.0044\,T + 1.2015 \tag{21}$$

$$l_{ij} = -0.0048\,T + 0.6055 \quad \& \quad k_{ij} = -0.0054\,T + 0.8462 \tag{22}$$

The optimized l_{ij} and k_{ij} parameters of the Chloroquine /sc-CO_2 system, along with the statistical parameters (*AARD%*, R_{adj} and *F-value*) of the SRK-EoS and PR-EoS were reported in Table 5.

Furthermore, the correlated and experimental solubility values at different temperatures (308, 318, 328 and 338 K) were shown in Fig. 7. As can be seen, both of the models can provide acceptable results at all the considered temperatures. However, according to the average of the obtained *AARD%* values (9.99 for PR-EoS and 10.7 for SRK-EoS) and R_{adj} values (0.993 for PR-EoS and 0.945 for SRK-EoS), it can be concluded that PR-EoS can more accurately correlate the solubility of Chloroquine in sc-CO_2. For better comparison, the parity plots of the experimental solubility data versus the

Table 5 Correlation results for solubility of Chloroquine in sc-CO_2, by PR and SRK combined with the vdW2 mixing rule.

Model	Parameter	T = 308 K	T = 318 K	T = 328 K	T = 338 K
PR- vdW2	k_{12}	−0.150	−0.194	−0.238	−0.282
	l_{12}	−0.218	−0.405	−0.592	−0.779
	AARD %	6.628	4.404	13.771	15.187
	F value	4745.7	7808.9	1963	416.2298
	R_{adj}	0.998	0.999	0.996	0.981
SRK- vdW2	k_{12}	−0.817	−0.871	−0.925	−0.979
	l_{12}	−0.873	−0.921	−0.969	−1.017
	AARD %	7.28	5.20	14.12	16.21
	F value	16.9	107.0	50.3	13.7
	R_{adj}	0.92	0.99	0.97	0.90

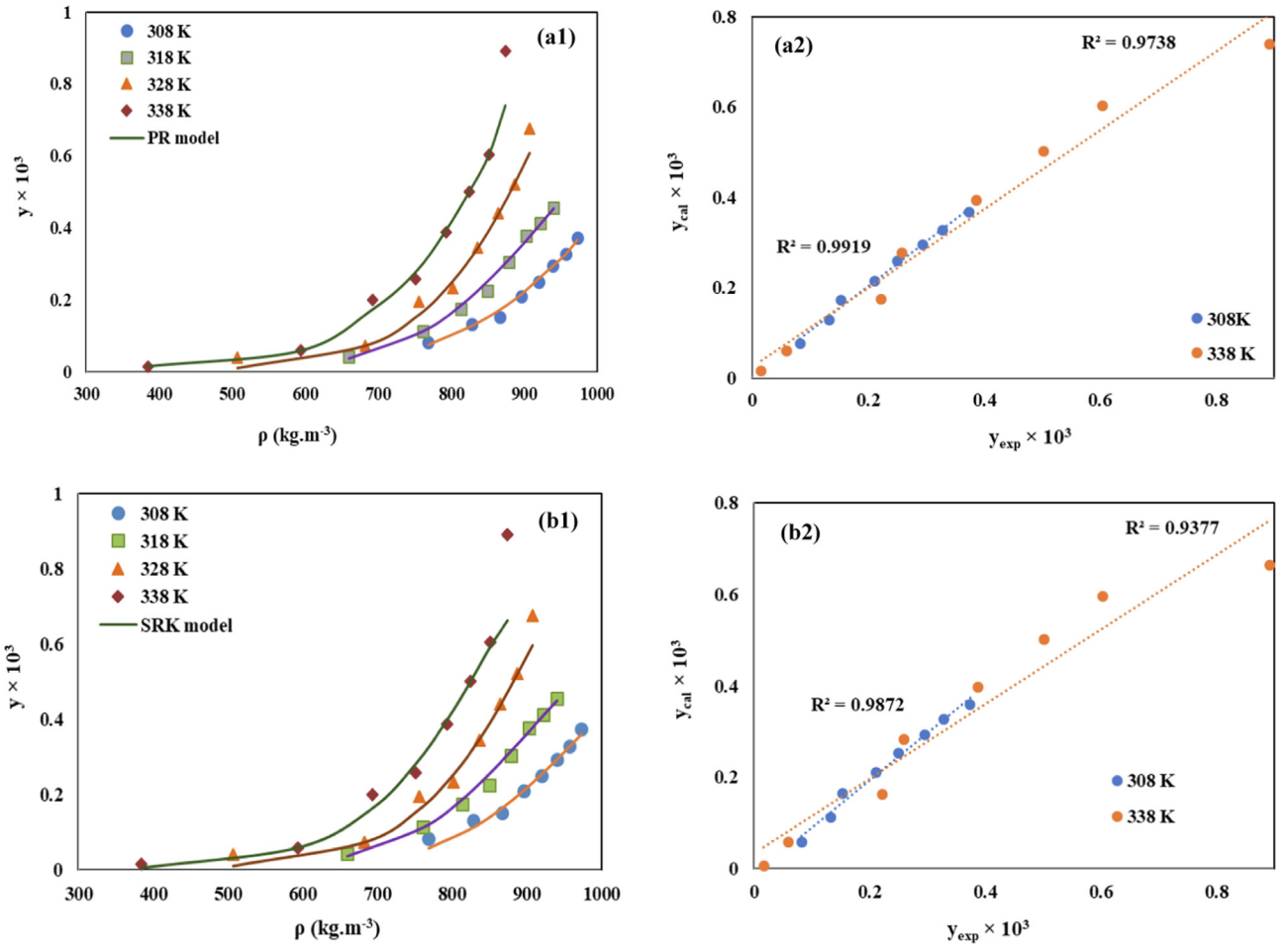

Fig. 7 Comparison of experimental (points) and calculated (line) solubility of Chloroquine in sc-CO_2,(left column) along with the related parity plot (right column), based on (a) PR-EoS, and (b) SRK-EoS models.

correlated ones at 308 K and 338 K were also demonstrated in Fig. 7. Higher precision of the PR-EoS model for correlation of the Chloroquine solubility is quite evident. Moreover, according to the obtained determination coefficients (R^2) of these plots, it is completely obvious that the accuracy of the correlation via both of the models reduces with increasing the temperature.

7.2.2. Expanded liquid theory (Modified Wilson's and UNIQUAC models)

For correlation of the Chloroquine solubility in sc-CO_2 based on the expanded liquid theory, its activity coefficient was determined via the modified Wilson's and UNIQUAC models. The capability of the modified Wilson's and UNIQUAC mod-

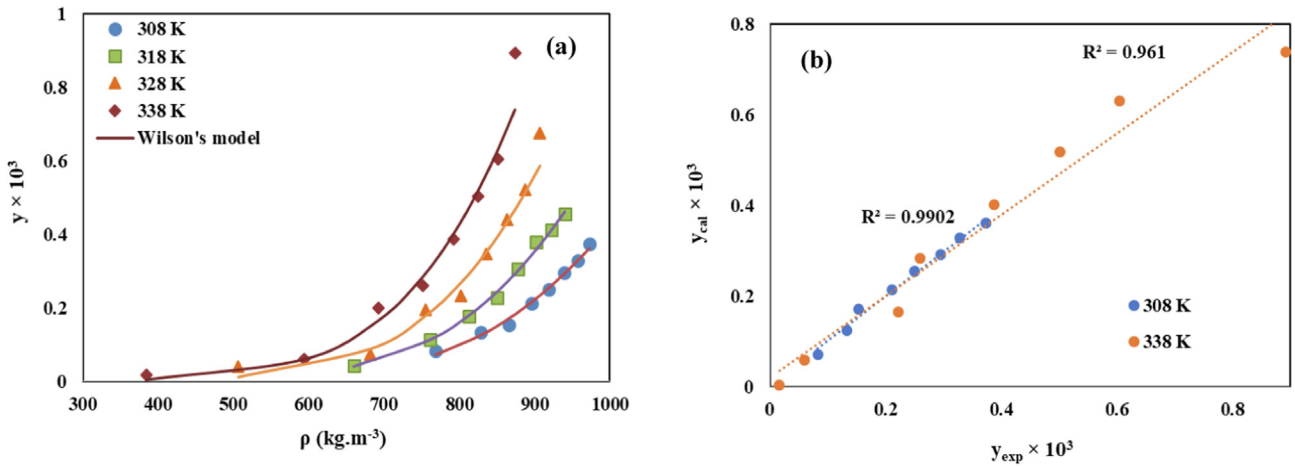

Fig. 8 (a) Comparison of experimental (points) and calculated (line) solubility of Chloroquine in sc-CO_2 based on the modified Wilson's model, (b) The related parity plot.

els to correlate the Chloroquine solubility was illustrated in Fig. 8 and Fig. 9, respectively.

Also, optimized regressed parameters of the modified Wilson's model (α, β, λ'_{12} and λ'_{21}) and UNIQUAC model (α_{12}, α_{21}, β_{12} and β_{21},), along with the obtained statistical parameters (*AARD%*, R_{adj}, and *F-value*) of each model for the Chloroquine /sc-CO_2 binary system were reported in Table 6 and Table 7, respectively. The volume *(r)*, and surface area *(q)* parameters of the UNIQUAC model were obtained as 13.089 and 10.117 for Chloroquine, and 1.296 and 1.261 for CO_2, respectively. Additionally, the interaction parameters of the Wilson's model (Λ_{12} and Λ_{21}) were calculated for each data point of Chloroquine /sc-CO_2 system. The values $\Lambda_{12}$and Λ_{21} parameters were calculated that, significant difference between these two parameters and higher value of Λ_{12}parameter in comparison with Λ_{21}, have been previously reported for complex solute molecules [13, 14, 82].

Low *AARD%* values (10.33 for Wilson and 12.3 for UNIQUAC models) and high R_{adj} values (0.97 for Wilson and 0.96 for UNIQUAC models), confirm the satisfactory precision of these models to correlate the Chloroquine solubility data. Good consistency between the calculated solubility values by the modified Wilson's and the UNIQUAC models and the reported experimental ones was also shown in the related parity plots shown in Fig. 8 and Fig. 9, respectively.

7.3. Comparison between the mentioned theoretical models and the empirical models used by Ponticelli and Moroni (2017)

As described in pervious sections, Pishnamazi et al. (2021) determined the supercritical solubility of Chloroquine and correlated the obtained experimental data via some empirical models (Kumar & Johnston (KJ), Mendez-Santiago-Teja (MST), Chrastil, Bartle *et al.*, and Garlapati &Madras models). In the continuation of this research, some thermodynamic models (PR-EOS, SRK-EoS, UNIQUAC, modified Wilson's models), and the ANN model were used in this work to correlate the supercritical solubility data of Chloroquine, reported by Ponticelli and Moroni (2017). Table 8 shows the comparison of these models in terms of their *AARD%* values.

As can be seen, the precision of the ANN model to correlate the Chloroquine supercritical solubility data is signifi-

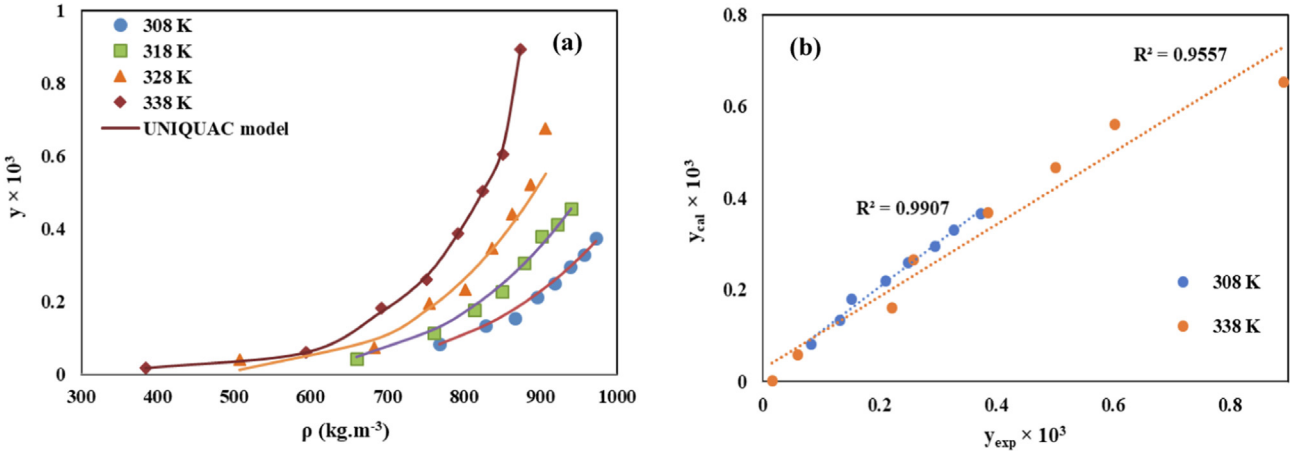

Fig. 9 (a) Comparison of experimental (points) and calculated (line) solubility of Chloroquine in sc-CO_2 based on the UNIQUAC model, (b) The related parity plot.

Table 6 Correlation results for solubility of Chloroquine in sc-CO_2 by modified Wilson's model.

Model	α	β	λ'_{12}	λ'_{21}	*AARD %*	*F value*	R_{adj}
Modified Wilson	-5.09×10^{-5}	2.85×10^{-4}	−1.38	18.49	10.33	254	0.97

Table 7 Correlation results for solubility of Chloroquine in sc-CO_2 by UNIQUAC model.

Model	α_{12}	α_{21}	β_{12}	β_{21}	*AARD %*	*F value*	R_{adj}
UNIQUAC	41.88	13.93	−0.45	−9.20	12.30	91.02	0.96

Table 8 Comparison of different models used to correlate Chloroquine solubility in $scCO_2$.

	Model	*AARD %*
Empirical models (reported by Pishnamazi *et al.* (Pishnamazi et al., 2021)	Kumar & Johnston (K-J)	12.3
	Mendez-Santiago-Teja (MST)	12.0
	Chrastil	13.3
	Bartle *et al*	13.0
	Garlapati &Madras	13.6
Cubic EoS- based models	PR-EoS	9.98
	SRK-EoS	10.70
Expanded liquid models	UNIQUAC	12.30
	Modified Wilson's	10.33
Intelligent model	Artificial neural network (ANN)	1.76

cantly more than the other ones. Also, despite the simplicity of the empirical models, their accuracy to fit the experimental Chloroquine solubility data is lower than the thermodynamic and intelligent models used in this work.

7.4. Molecular modeling

7.4.1. Estimated contact zones of Chloroquine

An analysis of the contact zones of Chloroquine showed that the most effective among them are the zones located near the N atom of pyridine and the hydrogen atom of the NH fragment. Therefore, it can be assumed that these atoms participate in the formation of a hydrogen bond during the formation of intermolecular contacts. The next in terms of the efficiency of contact formation, despite the low polarity, are the hydrogen atoms of the quinoline ring and the hydrogen atoms of the alkyl CH, CH_2, and CH_3 fragments. We may suggest the formation of lipophilic contacts of the groups with nonpolar atoms.

Indeed, consideration of the crystal fragment showed that the formation of a crystal is carried out with the participation of these fragments of the molecule. Fig. 10 shows the contact zones determined using the principles of VSEPR theory and 3D maps of Chloroquine electron density, estimated by the AlteQ orbital-free quantum chemical method.

7.4.2. Overlap zones and topological analysis of electron density of Chloroquine crystal fragment

Fig. 11a demonstrates the overlap zones of a molecule with the neighbors in a crystal fragment. Fig. 11b demonstrates the same zones in the molecule taken from the crystal fragment.

Indeed, the N of the pyridine forms a hydrogen bond with H of NH group, and the lipophilic nonpolar CH, CH_2, CH_3 fragments, as well as quinoline hydrogens, form intermolecular van der Waals interactions with each other (Fig. 11).

The topological analysis of the electron density of the crystal fragment showed that for the Chloroquine molecule, the formation of a significant number of weak lipophilic H...H and C...H contacts with neighboring molecules with an electron density of $\rho_{(3,-1)} = 0.0151 - 0.0288$ a.u. (e/Bohr^3) and $\rho_{(3,-1)} = 0.0287 - 0.0301$ a.u. respectively in (3,-1) bond critical points is observed. These intermolecular interactions are localized near the alkyl fragments, namely, near the CH, CH_2, CH_3 groups (Fig. 11b). In addition, one of the CH_3 groups is located near the pyridine ring of the quinoline fragment (Fig. 11b) with the electron density of $\rho_{(3,-1)} = 0.0714$ a.u. Weak π-stacking interactions are absent. Chlorine is in contact with the carbon atom of the pyridine ring, the value of the electron density at the critical point (3,-1) is low $\rho_{(3,-1)} = 0.0321$a.u. There are 4 N...H contacts, but they do not have a hydrogen-bonded character, because hydrogens belong to CH_3 groups, and moderate electron density values of $\rho_{(3,-1)} = 0.0365 - 0.0899$ a.u. are also observed in such N...H (3,-1) bond critical points. Only 2 N...H contacts, namely N(pyridine)...H—N(amine) and N—H(amine)...N (pyridine) contacts are typical hydrogen bonds with $\rho_{(3,-1)} = 0.1554$ a.u.

Thus, the compound dissolved in carbon dioxide crystallizes with the formation of intermolecular contacts due to the most pronounced contact zones which determine crystal structure. First of all, the N(pyridine)...H(NH fragment) hydrogen bond is formed; in addition, less effective lipophilic interactions of alkyl fragments are generated. Obviously, upon dissolution, the destruction of the crystal will be due to more vulnerable lipophilic interactions, and then by the destruction of the hydrogen N(pyridine)...H(NH fragment) bond.

7.4.3. Overlap zones and topological analysis of electron density of Chloroquine-CO_2 complexes

Overlap zones of Chloroquine-CO_2 complexes also in a good agreement with the predicted contact zones of the Chloroquine. It was found that, regardless of the mole fraction, the

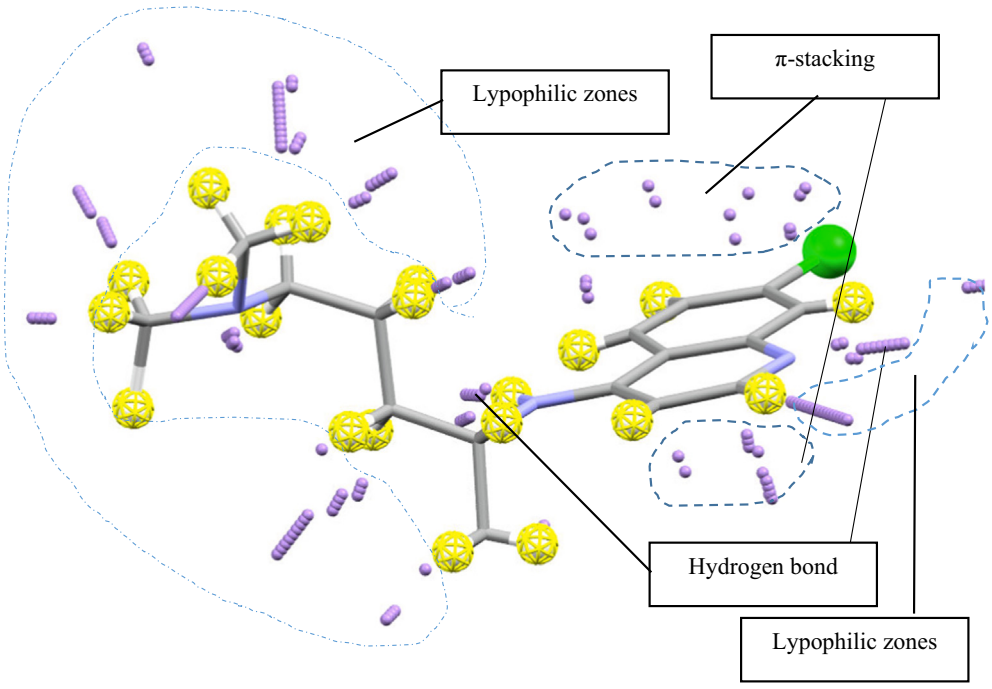

Fig. 10 Contact zones determined using principles of VSEPR theory and 3D maps of Chloroquine electron density estimated using AlteQ orbital-free quantum chemical method.

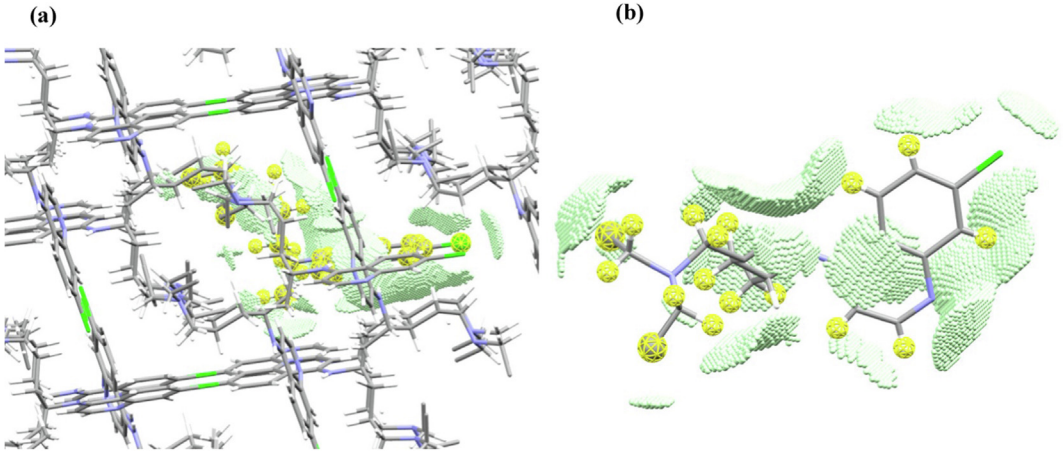

Fig. 11 Overlap zones of Chloroquine (a) a single molecule in the crystal fragment, and (b) a single molecule extracted from the crystal.

location of one CO_2 molecule is necessarily carried out near the H(NH) fragment, due to the formation of a O…H(NH) hydrogen bond (Fig. 12 a,b). The electron density value at the critical point doesn't exceed $\rho_{(3,-1)} = 0.0690$ a.u (the distance is 2.421 Å). In addition, the CO_2 carbon atom forms intermolecular interactions with the hydrogen atom of the benzene ring and the hydrogen atom of the CH_2 group (Fig. 12 a, b). The values of electron densities are not high, for example, in the complex with 1:1 composition and $1.64 \cdot 10^{-5}$ mol fraction, the values $\rho_{(3,-1)} = 0.0285$ a.u. and 0.0321 a.u. (the distances are 2.973 Å and 2.985 Å). The increase of the pressure and the number of CO_2 molecules increases the number of lypophilic contacts of $C(CO_2)$ with hydrogens of CH,CH_2,CH_3 groups (Fig. 12b). Then, the increase of number of explicit CO_2 molecules shows that the formation of π-stacking interactions of the CO_2 π -system and the quinoline ring with low electron density values of $\rho_{(3,-1)} = 0.0166$–0.0234 a.u. is possible (Fig. 12b).

Thus, the values at critical points show a less efficient interaction of CO_2 with Chloroquine, compared with interactions in the crystal, so the crystallization of Chloroquine from solution is simplified and in this case, the formation of a Chloroquine-CO_2 cocrystal is unlikely, which leads to the production of pure Chloroquine upon crystallization from a solution in CO_2.

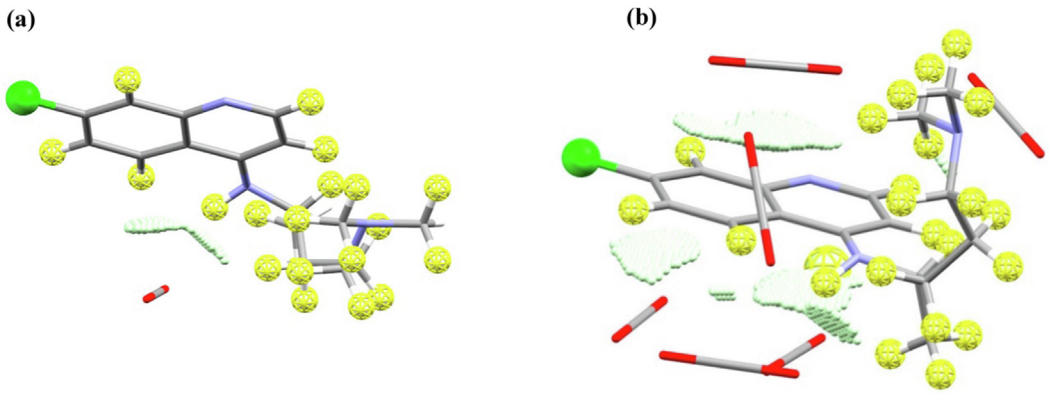

Fig. 12 Overlap zones of Chloroquine with CO_2 in their complexes obtained using MOPS algorithm, compositions are, (a) 1:1 (mole fraction is 1.64 10^{-5}), and (b) 1:6 (mole fraction is 8.92 10^{-4}).

8. Conclusion

It has been approved that pharmaceutical particles in micro/nano scale possess higher bioavailability and fewer side effects. Supercritical fluid (especially supercritical carbon dioxide (sc-CO_2) based processes are the novel and update approaches for this purpose. For design an efficient sc-CO_2 based process, the solubility of pharmaceutical substance should be measured at a wide range of temperatures and pressures. However, experimental solubility determination is costly, time consuming and complex process. Therefore, various theoretical methods have been developed for prediction the solubility of different components in sc-CO_2.

Chloroquine is a traditional antimalarial and antivirus medicine which is also prescribed for treatment the COVID-19 patients. Pishnamazi research team measured the Chloroquine solubility in sc-CO_2 in the range of 1.64×10^{-5} to 8.92×10^{-4} (in terms of mole fraction) at different pressures (120–400 bar) and temperatures (308–338 K). Also, they correlated the obtained solubility data via some commonly used empirical models (Kumar & Johnston (KJ), Mendez-Santiago-Teja (MST), Chrastil, Bartle *et al.*, and Garlapati &Madras models).

In the present study, two equation of states based models (Peng-Robinson (PR-EoS) and Soave-Redlich-Kowang (SRK-EoS)), two activity coefficient based models (modified Wilson's and UNIQUAC), and artificial neural network (ANN) model were applied for prediction the solubility of Chloroquine in sc-CO_2. Then, the predictability and accuracy of these methods was evaluated through calculating some statistical parameters such as average absolute relative deviation *(AARD %)*, adjusted correlation coefficient *(R_{adj})* and *F-value*. According to the obtained results, all of these models show acceptable accuracy for predicting the Chloroquine solubility in sc-CO_2. Among them, the ANN model is the most accurate with the lowest *AARD%* value of 1.76 % and the highest R_{adj} value of 0.999. The predicted solubility values by the ANN model are in the highest consistency with the experimental ones. Moreover, molecular modeling was performed to study the electronic structure of Chloroquine and identify the potential centers of intermolecular interactions during the dissolution process.

Declaration of Competing Interest

The authors declare that they have no known competing financial interests or personal relationships that could have appeared to influence the work reported in this paper.

Acknowledgements

This work was supported by Ministry of Science and Higher Education of Russia (grant FENU-2020-0019).

References

Abuzar, S.M., Hyun, S.-M., Kim, J.-H., Park, H.J., Kim, M.-S., Park, J.-S., Hwang, S.-J., 2018. Enhancing the solubility and bioavailability of poorly water-soluble drugs using supercritical antisolvent (SAS) process. Int. J. Pharm. 538, 1–13.

Ali Sajadian, S., Amani, M., Saadati Ardestani, N., Shirazian, S., 2022. Experimental Analysis and Thermodynamic Modelling of Lenalidomide Solubility in Supercritical Carbon Dioxide. Arabian J. Chem., 103821

Amani, Mitra et al, 2021. Experimental Optimization and Modeling of Supercritical Fluid Extraction of Oil from *Pinus gerardiana*. Chemical Engineering & Technology 44 (4), 578–588. https://doi.org/10.1002/ceat.202000347.

Amani, M., Saadati Ardestani, N., Majd, N.Y., 2021. Utilization of supercritical CO2 gas antisolvent (GAS) for production of Capecitabine nanoparticles as anti-cancer drug: Analysis and optimization of the process conditions. J. CO2 Util. 46, 101465.

Ardestani, N.S., Majd, N.Y., Amani, M., 2020. Experimental Measurement and Thermodynamic Modeling of Capecitabine (an Anticancer Drug) Solubility in Supercritical Carbon Dioxide in a Ternary System: Effect of Different Cosolvents. J. Chem. Eng. Data 65, 4762–4779.

Ardjmand, M., Mirzajanzadeh, M., Zabihi, F., 2014. Measurement and Correlation of Solid Drugs Solubility in Supercritical Systems. Chin. J. Chem. Eng. 22, 549–558.

Asiabi, H., Yamini, Y., Tayyebi, M., Moradi, M., Vatanara, A., Keshmiri, K., 2013. Measurement and correlation of the solubility of two steroid drugs in supercritical carbon dioxide using semi empirical models. J. Supercrit. Fluids 78, 28–33.

Assael, M.J., Trusler, J.M., Tsolakis, T.F., 1996. Thermophysical properties of fluids: an introduction to their prediction. World Scientific.

Bakhbakhi, Yousef, 2012. Neural network modeling of ternary solubilities of 2-naphthol in supercritical CO2: A comparative study. Mathematical and Computer Modelling 55 (7), 1932–1941. https://doi.org/10.1016/j.mcm.2011.11.051.

Bruce, J.M.P., Poling, E., O'Connell, J.P., 2001. Properties of Gases and Liquids. McGraw-Hill Education.

Ch, R., Madras, G., 2010. An association model for the solubilities of pharmaceuticals in supercritical carbon dioxide. Thermochim Acta 507–508, 99–105.

Chang, H., Morrell, D.G., 1985. Solubilities of methoxy-1-tetralone and methyl nitrobenzoate isomers and their mixtures in supercritical carbon dioxide. J. Chem. Eng. Data 30, 74–78.

Chim, R.B., de Matos, M.B.C., Braga, M.E.M., Dias, A.M.A., de Sousa, H.C., 2012. Solubility of Dexamethasone in Supercritical Carbon Dioxide. J. Chem. Eng. Data 57, 3756–3760.

Ciou, J.-M., Wang, B.-C., Su, C.-S., Liu, J.-J., Sheu, M.-T., 2017. Measurement of solid solubility of warfarin in supercritical carbon dioxide and recrystallization study using supercritical antisolvent process. Adv. Powder Technol. 29.

Coimbra, P., Duarte, C.M.M., Sousa, H.C.d., 2006. Cubic equation-of-state correlation of the solubility of some anti-inflammatory drugs in supercritical carbon dioxide. Fluid Phase Equilibria 239, 188–199.

Constantinou, L., Gani, R., 1994. New group contribution method for estimating properties of pure compounds. AIChE J. 40, 1697–1710.

Esfandiari, N., Sajadian, S.A., 2022. Experimental and modeling investigation of Glibenclamide solubility in supercritical carbon dioxide. Fluid Phase Equilib. 556, 113408.

Faress, F., Yari, A., Rajabi Kouchi, F., Safari Nezhad, A., Hadizadeh, A., Sharif Bakhtiar, L., Naserzadeh, Y., Mahmoudi, N., 2022. Developing an accurate empirical correlation for predicting anti-cancer drugs' dissolution in supercritical carbon dioxide. Sci. Rep. 12, 9380.

Ghoreishi, S.M., Heidari, E., 2013. Extraction of Epigallocatechin-3-gallate from green tea via supercritical fluid technology: Neural network modeling and response surface optimization. J. Supercrit. Fluids 74, 128–136.

Gillespie, R.J., 1963. The valence-shell electron-pair repulsion (VSEPR) theory of directed valency. J. Chem. Educ. 40, 295.

Gillespie, R.J., Nyholm, R.S., 1957. Inorganic stereochemistry. Q. Rev. Chem. Soc. 11, 339–380.

Grishina, M.A., Potemkin, V.A., 2019. Topological Analysis of Electron Density in Large Biomolecular Systems. Curr. Drug Discov. Technol. 16, 437–448.

Groom, C.R., Bruno, I.J., Lightfoot, M.P., Ward, S.C., 2016. The Cambridge Structural Database. Acta Crystallographica B 72, 171–179.

Gross, J., 2005. An equation-of-state contribution for polar components: Quadrupolar molecules. AIChE J. 51, 2556–2568.

Hezave, A., Aftab, S., Esmaeilzadeh, F., 2012. Solubility of sulindac in the supercritical carbon dioxide: Experimental and modeling approach. J. Supercrit. Fluids 68, 39–44.

Higashi, H., Iwai, Y., Arai, Y., 2001. Solubilities and diffusion coefficients of high boiling compounds in supercritical carbon dioxide. Chem. Eng. Sci. 56, 3027–3044.

Hojjati, M., Yamini, Y., Khajeh, M., Vatanara, A., 2007. Solubility of some statin drugs in supercritical carbon dioxide and representing the solute solubility data with several density-based correlations. J. Supercrit. Fluids 41, 187–194.

Hosseini, M.H., Alizadeh, N., Khanchi, A.R., 2010. Solubility analysis of clozapine and lamotrigine in supercritical carbon dioxide using static system. J. Supercrit. Fluids 52, 30–35.

Immirzi, A., Perini, B., 1977. Prediction of density in organic crystals. Acta Crystallographica Section A 33, 216–218.

Kankala, R.K., Zhang, Y.S., Wang, S.B., Lee, C.H., Chen, A.Z., 2017. Supercritical Fluid Technology: An Emphasis on Drug Delivery and Related Biomedical Applications. Adv. Healthcare Mater. 6.

Karimi Sabet, J., Ghotbi, C., Dorkoosh, F., Striolo, A., 2012. Solubilities of acetaminophen in supercritical carbon dioxide with and without menthol cosolvent: Measurement and correlation. Scientia Iranica 19, 619–625.

Kennedy, J., 2011. Particle swarm optimization, Encyclopedia of machine learning. Springer, pp. 760–766.

Khamda, M., Hosseini, M.H., Rezaee, M., 2013. Measurement and correlation solubility of cefixime trihydrate and oxymetholone in supercritical carbon dioxide (CO2). J. Supercrit. Fluids 73, 130–137.

Lashkarbolooki, M., Vaferi, B., Rahimpour, M.R., 2011. Comparison the capability of artificial neural network (ANN) and EOS for prediction of solid solubilities in supercritical carbon dioxide. Fluid Phase Equilib. 308, 35–43.

Liu, J., Cao, R., Xu, M., Wang, X., Zhang, H., Hu, H., Li, Y., Hu, Z., Zhong, W., Wang, M., 2020. Hydroxychloroquine, a less toxic derivative of chloroquine, is effective in inhibiting SARS-CoV-2 infection in vitro. Cell Discovery 6, 16.

Loubna, N., Bensaad, S., Bensetiti, Z., 2014. Modeling the Solubility of Dihydroxybenzoic Acid and Methylbenzoic Acid Isomers in Supercritical Carbon Dioxide. Int. J. Thermodyn. 17.

Marrero, J., Gani, R., 2001. Group-contribution based estimation of pure component properties. Fluid Phase Equilibr 183–184, 183–208.

Morales-Díaz, C., Cabrera, A., Fuente, J., Mejia, A., 2021. Modelling of solubility of vitamin K3 derivatives in supercritical carbon dioxide using cubic and SAFT equations of state. J. Supercrit. Fluids 167, 105040.

Najmi, M., Ayari, M.A., Sadeghsalehi, H., Vaferi, B., Khandakar, A., Chowdhury, M.E.H., Rahman, T., Jawhar, Z.H., 2022. Estimating the Dissolution of Anticancer Drugs in Supercritical Carbon Dioxide with a Stacked Machine Learning Model. Pharmaceutics 14, 1632.

Narayan, R.C., Dev, J.V., Madras, G., 2015. Experimental determination and theoretical correlation for the solubilities of dicarboxylic acid esters in supercritical carbon dioxide. J. Supercrit. Fluids 101, 87–94.

Nasri, L., 2018. Modified Wilson's Model for Correlating Solubilities in Supercritical Fluids of Some Polycyclic Aromatic Solutes. Polycyclic Aromat. Compd. 38, 244–256.

Nasri, L., Bensetiti, Z., Bensaad, S., 2012. Correlation of the Solubility of Some Organic Aromatic Pollutants in Supercritical Carbon Dioxide Based on the UNIQUAC Equation. Energy Procedia 18, 1261–1270.

Nasri, L., Bensaad, S., Bensetiti, Z., 2013. Correlation and Prediction of the Solubility of Solid Solutes in Chemically Diverse Supercritical Fluids Based on the Expanded Liquid Theory. Adv. Chem. Eng. Sci. 3, 255.

Palko, N., Grishina, M., Potemkin, V., 2021. Electron Density Analysis of SARS-CoV-2 RNA-Dependent RNA Polymerase Complexes. Molecules (Basel, Switzerland) 26.

Peng, D.-Y., Robinson, D.B., 1976. A New Two-Constant Equation of State. Ind. Eng. Chem. Fundam. 15, 59–64.

Pishnamazi, M., Zabihi, S., Jamshidian, S., Borousan, F., Hezave, A. Z., Shirazian, S., 2020. Thermodynamic modelling and experimental validation of pharmaceutical solubility in supercritical solvent. J. Mol. Liq. 319, 114120.

Pishnamazi, M., Zabihi, S., Jamshidian, S., Hezaveh, H.Z., Hezave, A. Z., Shirazian, S., 2020. Measuring solubility of a chemotherapy-anti cancer drug (busulfan) in supercritical carbon dioxide. J. Mol. Liq. 317, 113954.

Pishnamazi, M., Zabihi, S., Jamshidian, S., Borousan, F., Hezave, A. Z., Marjani, A., Shirazian, S., 2021. Experimental and thermodynamic modeling decitabine anti cancer drug solubility in supercritical carbon dioxide. Sci. Rep. 11, 1075.

Pishnamazi, M., Hosseini, S., Zabihi, S., Borousan, F., Zeinolabedini Hezave, A., Marjani, A., Shirazian, S., 2021. Chloroquine (anti-malaria medication with anti SARS-CoV activity) solubility in supercritical carbon dioxide. J. Mol. Liq. 322, 114539.

Pitchaiah, K.C., Lamba, N., Sivaraman, N., Madras, G., 2018. Solubility of trioctylmethylammonium chloride in supercritical carbon dioxide and the influence of co-solvents on the solubility behavior. J. Supercrit. Fluids 138, 102–114.

Pitchaiah, K.C., Lamba, N., Deepitha, J., Mohapatra, P.K., Madras, G., Sivaraman, N., 2019. Experimental measurements and correlation of the solubility of N, N-dialkylamides in supercritical carbon dioxide. J. Supercrit. Fluids 143, 162–170.

Ponticelli, C., Moroni, G., 2017. Hydroxychloroquine in systemic lupus erythematosus (SLE). Expert Opin. Drug Safety 16, 411–419.

Potemkin, V.A., Grishina, M.A., 2008. A new paradigm for pattern recognition of drugs. J. Comput. Aided Mol. Des. 22, 489–505.

Potemkin, V., Grishina, M., 2018. Electron-based descriptors in the study of physicochemical properties of compounds. Comput. Theor. Chem. 1123, 1–10.

Potemkin, V., Grishina, M., 2021. The Complementarity Principle-One More Step towards Analytical Docking on the Example of Dihydrofolate Reductase Complexes. Life (Basel) 11.

Prausnitz, J.M., Lichtenthaler, R.N., de Azevedo, E.G., 1998. Molecular thermodynamics of fluid-phase equilibria. Pearson Education.

Reddy, S.N., Madras, G., 2012. An association and Wilson activity coefficient model for solubilities of aromatic solid pollutants in supercritical carbon dioxide. Thermochim Acta 541, 49–56.

Reddy, S.N., Madras, G., 2013. Experimental determination and activity coefficient based models for mixture solubilities of nitrophenol isomers in supercritical carbon dioxide. J. Supercrit. Fluids 79, 2–10.

Rezaei, T., Nazarpour, V., Shahini, N., Bahmani, S., Shahkar, A., Abdihaji, M., Ahmadi, S., Shahdost, F.T., 2022. A universal methodology for reliable predicting the non-steroidal anti-inflammatory drug solubility in supercritical carbon dioxide. Sci. Rep. 12, 1043.

Rimac, H., Grishina, M.A., Potemkin, V.A., 2020. Electron density analysis of CDK complexes using the AlteQ method, Future. Med. Chem. 12, 1387–1397.

Saadati Ardestani, N., Amani, M., Moharrery, L., 2020. Determination of Anthraquinone Violet 3RN solubility in supercritical carbon dioxide with/without co-solvent: Experimental data and modeling (empirical and thermodynamic models). Chem. Eng. Res. Des. 159, 529–542.

Shchelokov, A., Palko, N., Potemkin, V., Grishina, M., Morozov, R., Korina, E., Uchaev, D., Krivtsov, I., Bol'shakov, O., chelokov et al., Langmuir 2019,. Adsorption of Native Amino Acids on Nanocrystalline TiO2: Physical Chemistry, QSPR, and Theoretical Modeling. Langmuir 35, 538–550.

Shojaee, S.A., Rajaei, H., Hezave, A.Z., Lashkarbolooki, M., Esmaeilzadeh, F., 2013. Experimental measurement and correlation for solubility of piroxicam (a non-steroidal anti-inflammatory drugs (NSAIDs)) in supercritical carbon dioxide. J. Supercrit. Fluids 80, 38–43.

Soave, G., 1972. Equilibrium constants from a modified Redlich-Kwong equation of state. Chem. Eng. Sci. 27, 1197–1203.

Sodeifian, G., Ardestani, N., Razmimanesh, F., Seyed Ali, S., 2020. Experimental and thermodynamic analyses of supercritical CO2-Solubility of minoxidil as an antihypertensive drug. Fluid Phase Equilibr 522.

Sodeifian, G., Saadati Ardestani, N., Razmimanesh, F., Sajadian, S. A., 2020. Experimental and thermodynamic analyses of supercritical CO2-Solubility of minoxidil as an antihypertensive drug. Fluid Phase Equilib. 522, 112745.

Sodeifian, G., Razmimanesh, F., Saadati Ardestani, N., Sajadian, S. A., 2020. Experimental data and thermodynamic modeling of solubility of Azathioprine, as an immunosuppressive and anticancer drug, in supercritical carbon dioxide. J. Mol. Liq. 299, 112179.

Suleiman, D., Estévez, L.A., Pulido, J.C., García, J.E., Mojica, C., 2005. Solubility of anti-inflammatory, anti-cancer, and anti-HIV drugs in supercritical carbon dioxide. J. Chem. Eng. Data 50, 1234–1241.

Türk, M., 2016. Polymorphic properties of micronized Mefenamic acid, Nabumetone, Paracetamol and Tolbutamide produced by Rapid Expansion of Supercritical Solutions (RESS). J. Supercrit. Fluids 116.

Vaferi, B., Karimi, M., Azizi, M., Esmaeili, H., 2013. Comparison between the artificial neural network, SAFT and PRSV approach in obtaining the solubility of solid aromatic compounds in supercritical carbon dioxide. J. Supercrit. Fluids 77, 44–51.

Van der Waals, J.D., 1873. Over de Continuiteit van den Gas-en Vloeistoftoestand (On the Continuity of the Gas and Liquid State). University of Leiden.

Wang, S.-W., Chang, S.-Y., Hsieh, C.-M., 2021. Measurement and modeling of solubility of gliclazide (hypoglycemic drug) and captopril (antihypertension drug) in supercritical carbon dioxide. J. Supercrit. Fluids 174, 105244.

Xiang, S.-T., Chen, B.-Q., Kankala, R.K., Wang, S.-B., Chen, A.-Z., 2019. Solubility measurement and RESOLV-assisted nanonization of gambogic acid in supercritical carbon dioxide for cancer therapy. J. Supercrit. Fluids 150, 147–155.

Yamini, Y., Hojjati, M., Kalantarian, P., Moradi, M., Esrafili, A., Vatanara, A., 2012. Solubility of capecitabine and docetaxel in supercritical carbon dioxide: Data and the best correlation. Thermochim Acta 549, 95–101.

Yamini, Y., Moradi, M., 2011. Measurement and correlation of antifungal drugs solubility in pure supercritical CO2 using semiempirical models. J. Chem. Thermodyn. 43, 1091–1096.

Yang, G., Li, Z., Shao, Q., Feng, N., 2017. Measurement and correlation study of silymarin solubility in supercritical carbon dioxide with and without a cosolvent using semi-empirical models and back-propagation artificial neural networks. Asian J. Pharm. Sci. 12, 456–463.

Zabihi, S., Rahnama, Y., Sharafi, A., Borousan, F., Zeinolabedini Hezave, A., Shirazian, S., 2020. Experimental Solubility Measurements of Fenoprofen in Supercritical Carbon Dioxide. J. Chem. Eng. Data 65, 1425–1434.

Zabihi, S., Khoshmaram, A., Pishnamazi, M., Borousan, F., Hezave, A.Z., Marjani, A., Pelalak, R., Kurniawan, T.A., Shirazian, S., 2021. Thermodynamic study on solubility of brain tumor drug in supercritical solvent: Temozolomide case study. J. Mol. Liq. 321, 114926.

Zabihi, S., Jamshidian, S., Borousan, F., Zeinolabedini Hezave, A., Pishnamazi, M., Marjani, A., Shirazian, S., 2021. Measuring salsalate solubility in supercritical carbon dioxide: Experimental and thermodynamic modelling. J. Chem. Thermodyn. 152, 106271.

Zeinolabedini Hezave, A., Esmaeilzadeh, F., 2012. Solubility Measurement of Diclofenac Acid in the Supercritical CO2. J. Chem. Eng. Data 57, 1659–1664.

Zeinolabedini Hezave, A., Khademi, M.H., Esmaeilzadeh, F., 2012. Measurement and modeling of mefenamic acid solubility in supercritical carbon dioxide. Fluid Phase Equilib. 313, 140–147.

Zhan, S., Zhao, Q., Chen, S., Wang, J., Liu, Z., Chen, C., 2014. Solubility and Partition Coefficients of 5-Fluorouracil in ScCO2 and ScCO2/Poly(l-lactic acid). J. Chem. Eng. Data 59, 1158–1164.

Zhao, Y., Wang, W., Liu, W., Zhu, J., Pei, X., 2020. Density-based UNIFAC model for solubility prediction of solid solutes in supercritical fluids. Fluid Phase Equilib. 506, 112376.